COMPARATIVE ANALYSIS OF MECHANICAL PROPERTIES OF INCONEL AND MARTENSITIC STAINLESS STEEL JOINTS ACHIEVED BY TUNGSTEN INERT GAS WELDING

A. Ramaswamy[1*], G. Ashok[1], B. Prasanna Nagasai[2]

[1*] Department of Mechanical Engineering, Sasi Institute of Technology and Engineering, Tadepalligudem, India
[2]Centre for Sustainable Materials and Surface Metamorphosis, Department of Mechanical Engineering, Chennai Institute of Technology, India
*Corresponding author's e-mail address: ramaswamy@sasi.ac.in

ABSTRACT

This work provides a detailed comparative study on the mechanical performance and microstructural features of dissimilar joints produced by Tungsten Inert Arc welding (TIG) between Inconel 718 and AISI 410 martensitic stainless steel. Welding was performed on 2 mm thick sheets of both alloys using optimized conditions: 80 A current, 12.1 V voltage, 60 cm/min travel speed. Microstructural evaluation revealed contrasting solidification patterns, with Inconel 718 exhibiting Laves phase precipitation within dendritic networks, while AISI 410 displayed coarse dendrites interspersed with sulfur-based inclusions. Vickers microhardness analysis indicated a non-uniform distribution across the weldment. The highest hardness (410 HV) occurred in the AISI 410 heat-affected zone (HAZ) due to martensitic transformation, whereas the Inconel 718 base metal and fusion zone recorded 267±3 HV and 264±5 HV, respectively. Tensile testing demonstrated an ultimate tensile strength of 461±2 MPa, a yield strength of 273 MPa, and an elongation of 17.95±0.8% for the welded joint.

KEYWORDS: TIG welding, Vickers microhardness, martensitic stainless steel, tensile, Inconel

1. INTRODUCTION

The rapid evolution of aerospace, power generation, and petrochemical sectors has significantly increased the demand for advanced materials capable of operating under extreme service conditions – such as elevated temperatures, corrosive environments, and high mechanical loads. Among the material classes employed in these critical areas, nickel-based superalloys (notably INCONEL 718) and martensitic stainless steels have gained prominence due to their outstanding mechanical strength, corrosion resistance, and thermal stability. For these materials to perform effectively in engineering applications, robust joining techniques are essential, with Gas Tungsten Arc Welding (GTAW or TIG welding) being one of the most widely used methods for producing precision welds in such high-performance alloys [1-2]. INCONEL 718, a precipitation-hardened nickel-chromium-iron alloy, is extensively used in aerospace and industrial applications owing to its exceptional strength retention up to 700 °C, excellent resistance to corrosion, and superior creep properties. The alloy's high strength is primarily attributed to the precipitation of γ' ($Ni_3(Al,Ti)$) and γ'' (Ni_3Nb) phases, enabling impressive mechanical performance with ultimate tensile strengths above 827 MPa and yield strengths near 414 MPa at room temperature. However, welding this alloy poses considerable challenges due to issues such as solidification cracking, grain boundary liquation, and the dissolution of strengthening precipitates within the heat-affected zone (HAZ), which can compromise weld integrity and mechanical properties [1-2].

Martensitic stainless steels form another critical category of engineering materials, widely employed in high-strength applications where good hardness and moderate corrosion resistance are required. Their martensitic transformation during cooling produces a strong, hard microstructure, which can be further optimized by heat treatment. Nevertheless, welding these steels introduces its own complexities, including susceptibility to hydrogen-induced cracking, formation of untempered martensite in the HAZ, and possible reductions in corrosion resistance due to carbide precipitation and microstructural changes during thermal cycling [3]. TIG welding is often the preferred method for joining both INCONEL 718 and martensitic stainless steels, as it offers precise heat control, superior arc stability, and minimal contamination through inert gas shielding. This process

Date of submission/acceptance: 03.09.2025/15.12.2025
https://doi.org/10.35219/awet.2025.14

allows for the production of high-quality welds with excellent mechanical properties when parameters are properly optimized. However, welding variables significantly influence the resulting microstructure and performance, making it essential to establish clear relationships between processing conditions, microstructural development, and mechanical behaviour for each alloy system [4].

Recent studies have continued to emphasize the distinct metallurgical challenges involved in welding Inconel 718, particularly using TIG (GTAW) and in dissimilar joints with stainless steels like AISI 410. Górka et al. [5] conducted an in-depth microstructural and hardness analysis of TIG-welded butt joints made from thin Inconel 718 sheets with varying welding energy (45–80 J/mm). Their results showed that weld quality and mechanical performance, including hardness, are highly sensitive to thermal energy input, with higher energy increasing weld and HAZ widths and shifting grain morphology in the fusion zone from elongated to more equiaxed dendritic structures. The weld region displayed higher hardness compared to the HAZ and base material, attributed to precipitation of carbides, intermetallics, and eutectics along grain boundaries and in interdendritic regions, which significantly affect post-weld mechanical behaviour, including susceptibility to cracking. Complementing this, Yelamasetti et al. [6] investigated TIG weldments of Inconel 718 and SS316L under elevated temperatures and confirmed that optimizing welding parameters improves both fusion quality and high-temperature mechanical performance.

Reviews and additional studies further reinforce these findings. Kumar [7] highlighted that GTAW dissimilar welding of Inconel 718 and ferritic/martensitic stainless steels such as SS410 can produce high microhardness and tensile strength in the joint region, but cautioned that careful control of process parameters is necessary to minimize brittle intermetallic formation. Research by Hejripour et al. [8] and Shehbaz et al. [9] examined consumable selection, interdiffusion phenomena, and mechanical testing in dissimilar weldments, emphasizing the critical interplay between microstructural evolution and mechanical performance at Ni-based superalloy–martensitic stainless steel interfaces. Across these studies, fractographic, SEM, and X-ray analyses consistently underscore the importance of controlling heat input to manage microstructural development, precipitation behaviour, and residual stress, ultimately enhancing weld joint reliability and performance.

The microstructural evolution during TIG welding differs markedly between these two materials. For INCONEL 718, challenges include Laves phase formation, delta phase precipitation, and changes in strengthening phases caused by repeated dissolution and reprecipitation. In contrast, martensitic stainless steels face issues such as carbon migration, brittle phase formation, and residual stresses resulting from martensitic transformation. A thorough understanding of these metallurgical phenomena is essential for designing suitable welding procedures and post-weld heat treatments [10].

Recent developments in welding technologies—such as advanced heat input control, magnetic arc oscillation, and optimized shielding gas mixtures—have improved weld quality for both material systems. Nevertheless, their effectiveness varies significantly because of differences in thermal properties, phase transformation behaviours, and solidification dynamics between INCONEL 718 and martensitic steels. This underlines the need for systematic comparative evaluations to identify the relative advantages and limitations of TIG welding for each alloy.

2. EXPERIMENTS

The base metal (BM) taken in this investigation was Inconel 718 and AISI 410 alloy of thin sheets of 2 mm thickness. The chemical composition of the base metal was checked by optical spectrometer. Mechanical properties of the base metal were evaluated using universal testing machine and micro hardness tester is used in this investigation.

Table 1 shows the chemical composition of base metal. Table 2 shows the mechanical properties of the base metal. The welding equipment and setup is shown in figure 1.

Table 1. Chemical composition of base materials, wt. [%]

Material	C	Si	Mn	Cr	Mo	Ni	P	S	Fe
IN 718	0.12	1.15	1.80	0.15	0.15	0.15	0.025	0.025	Bal
MSS 410	0.15	1	1	13.5	0.04	0.75	0.04	0.03	Bal

Table 2. Mechanical properties of base materials

Material	Yield strength [MPa]	Ultimate tensile strength [MPa]	Elongation in a gauge length of mm [%]
IN 718	335 ± 10	730 ± 10	60 ± 2
MSS 410	290 ± 5	465 ± 5	33 ± 3

Fig. 1. Welding system employed in the experimental programme

Table 3. TIG welding parameters

Parameters	Values
Current [A]	80
Voltage [V]	12.1
Travel speed [cm/min]	60
100% Ar [l/min]	15

The welding process parameters chosen for welding these sheets are shown in table 3. The shielding gas used was Argon with a flow rate of 15 lit/min. Contact tip to work piece distance (CTWD) was maintained as 15 mm. The image of the welded joints is shown in the figure 2. The heat input was calculated using the following equation:

$$\text{HI (kJ/mm)} = \frac{\eta \text{ x V x I x 60}}{\text{S x 1000}} \qquad (1)$$

where V is the arc voltage in volts, I is the average welding current in [A], S is the welding speed in [mm/min] and η is the thermal efficiency = 0.65.

Fig. 2. Image of the welded joint

3. RESULTS AND DISCUSSION

3.1. Macro and Microstructure

3.1.1. Macrostructure

Figure 3 shows the macrostructure of the joint. Figure 4 shows the schematic representation of the macrostructure of dissimilar joint. Understanding the characteristics, behaviour, and performance of materials, can be gained through the analysis and characterization of macrostructures. Using methods such as optical microscopy, visual inspection is frequently the first step in macrostructure study. This makes it possible to see characteristics like inclusions, cracks, porosity, and grain boundaries. In order to help characterize materials microstructure, optical microscopy offers important information regarding the spatial arrangement of grains and phases within the material.

3.1.2. Microstructure

Figure 5h and 5i show the optical micrograph of fusion zone with TIG welding process. The fusion zone solidifies in cast dendritic mode. Increase in heat input shows significant increase in dendritic grain growth. It refers to the optimum heat input supplied to the weld pool. Increase in heat input results in the evolution of coarse dendritic grains in fusion zone. The fusion zone showed well developed dendritic structure with large inter-dendritic spacings at high heat input. Figures 5d and 5f shows the micrographs of the fusion zone near the Inconel 718 side.

The microstructure of the fusion zone near the Inconel 718 shows laves phases (Fig. 5f). The laves phase appears to be evolved in the form of thick continuous film decorating the area of dendrite core. Similarly, the microstructure of the fusion zone near

the Inconel 718 shows coarse dendritic structure which are growing in the interface of Inconel 718 side. Figures 5g and 5i show the micrographs of the fusion zone near the AISI 410 side. The microstructure of the fusion zone near the AISI 410 shows coarse dendritic with more amount of sulphur inclusion particles in joint (Fig. 5e).

The sulphur inclusion particles were observed to be coarser and interconnected in the fusion zone near the AISI 410 side. The microstructure of the fusion zone near the AISI 410 shows coarse dendritic with more amount of sulphur inclusion particles in joint (Fig. 5e).

The sulphur inclusion particles were observed to be coarser and interconnected in the fusion zone.

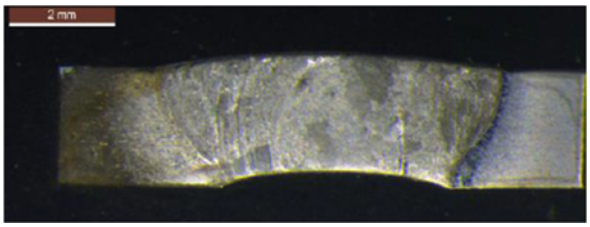

Fig. 3. Macrostructure of Inconel 718 – 410 MSS dissimilar joints

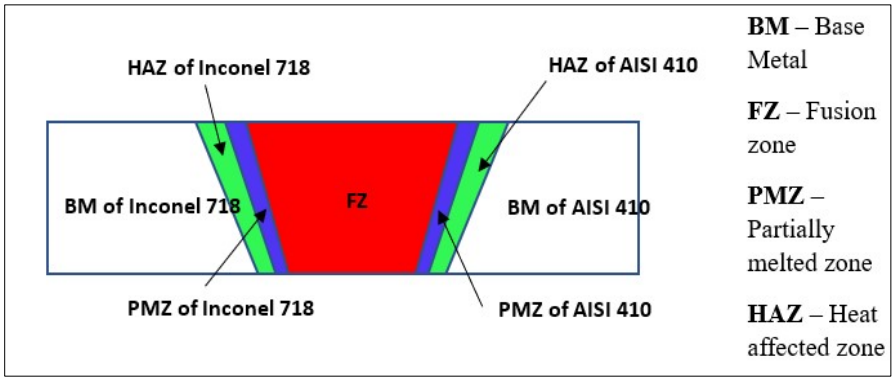

Fig. 4. Schematic diagram of the macrostructure of dissimilar joint

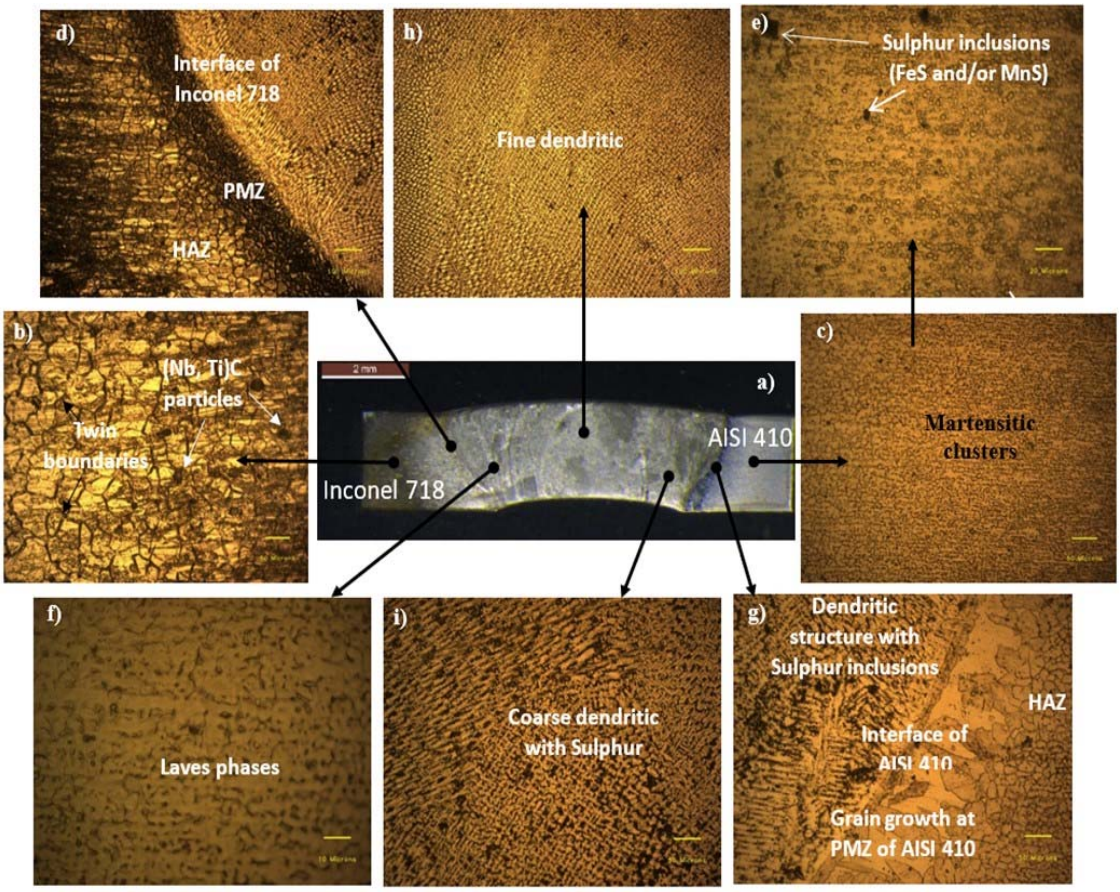

Fig. 5. Macro and microstructure of the welded joint

3.2. Mechanical Properties

3.2.1. Microhardness

Hardness testing is crucial for assessing how well components can endure and function in particular applications. The hardness of a welded sample is influenced by the different material phases and the microstructure that forms during the welding process. This research involved conducting Vickers micro-hardness tests on weldments in three distinct areas: the fusion zone, the base metal, and the heat-affected zone.

The study focused on measuring Vickers microhardness at various points around the centre of the weld around the weld centre. Table 4 presents the hardness values for both weldments. In the heat-affected zone of AISI 410, TIG weldments showed higher hardness levels compared to the base metal and fusion zones. The peak hardness near AISI 410 was linked to the formation of martensite, which is known for its high carbon content. The increased hardness observed in autogenous GTA welding, with and without flux injection, compared to previous research by (Manikandan et al., 2016) might be attributed to the fine-grained dendritic microstructure in the weld zone. Additionally, Shit et al. [13] discovered that fusion zones with fine-grained, columnar, dendritic structures tend to provide superior hardness values compared to equiaxed ones. The results clearly indicate that the heat-affected zone (HAZ) of AISI 410 in both GTA weldments exhibited higher hardness levels than other zones.

For Inconel 718, the HAZ showed hardness values of 247 ± 4 HV in TIG weldments. Notably, the table suggests that the hardness values for both welding techniques are quite similar.

Regarding the hardness of the parent metal, Inconel 718 and AISI 410 showed values of 267 ± 3 HV for TIG, while AISI 410 alone displayed 164 ± 5 HV.

Furthermore, slightly reduced hardness values were observed in the fusion zone and base metal, likely due to the application of multiple passes and the presence of an austenitic matrix with dendritic morphologies in this welding process.

Table 4. Average microhardness of Inconel 718 and AISI 410 joints

Process	Inconel 718	HAZ of IN718	Fusion zone	HAZ AISI 410	AISI 410
TIG	267 ± 3	247 ± 4	264 ± 5	410	164 ± 5

Hardness testing is a crucial technique for evaluating the performance of components in their designated applications. It depends on the presence of different material phases and the microstructure created during welding to determine the hardness value of the welded sample [11]. This research employed Vickers micro-hardness testing to evaluate weldments produced using TIG methods across three areas: the fusion zone, the base metal, and the heat-affected zone. During the study, the Vickers microhardness of welded specimens was assessed at various points around the weld centre. Table 4 presents the hardness values for both weldments. In the heat-affected zone of AISI 410, TIG weldments showed higher hardness levels compared to the base metal and fusion zones. The peak hardness near AISI 410 was linked to the formation of martensite, which is known for its high carbon content. The increased hardness observed in autogenous GTA welding, with and without flux injection, compared to previous research by Manikandan et al. [12] might be attributed to the fine-grained dendritic microstructure in the weld zone. Additionally, Shit et al., [13] discovered that fusion zones with fine-grained, columnar, dendritic structures tend to provide superior hardness values compared to equiaxed ones.

The results clearly indicate that the heat-affected zone (HAZ) of AISI 410 in both GTA weldments exhibited higher hardness levels than other zones. For Inconel 718, the HAZ showed hardness values of 247 ± 4 HV in TIG weldments. Notably, the table suggests that the hardness values for both welding techniques are quite similar.

Regarding the hardness of the parent metal, Inconel 718 and AISI 410 showed values of 267 ± 3 HV for TIG, while AISI 410 alone displayed 164 ± 5 HV. Furthermore, slightly reduced hardness values were observed in the fusion zone and base metal, likely due to the application of multiple passes and the presence of an austenitic matrix with dendritic morphologies in both welding methods.

3.2.2. Tensile Properties

The tensile testing revealed that Inconel 718 had a tensile strength of 730 ± 10 MPa, while AISI 410 had a tensile strength of 465 ± 5 MPa. Fractures occurred in the AISI 410 base metal during the tensile evaluation as shown in the figure 6. Table 5 shows the mechanical properties of Inconel 718 and AISI 410 dissimilar joints. After welding and cooling, the austenitic weld metal's cap area transformed into martensite, likely due to the denser nature of austenite compared to martensite, resulting in volume expansion. This transformation may have caused the weld metal to reach room temperature under compressive stress.

Tensile measurements showed that the fusion zone exhibited greater strength than the AISI 410 base metal. In TIG joints, the ultimate tensile strength was 461 MPa.

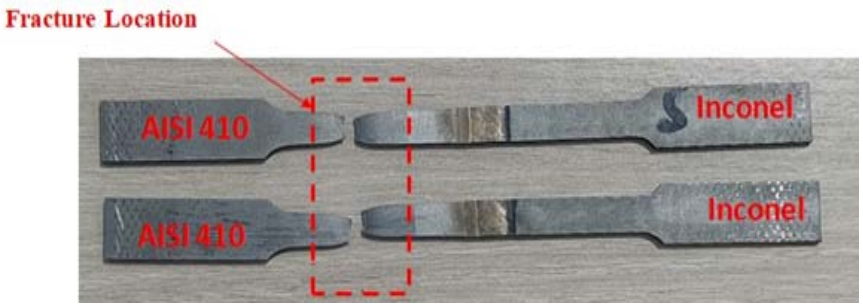

Fig. 6. Specimens subjected to tensile testing

Tensile testing of TIG-welded joints revealed notable differences between Inconel 718 and martensitic stainless steel weldments. The base Inconel 718 material recorded an ultimate tensile strength of 827 ± 15 MPa, whereas welded joints exhibited a maximum strength of 730 ± 10 MPa, while the welded joints achieve 496 ± 22 MPa, resulting in a joint efficiency of approximately 70%. This drop in strength was mainly attributed to the development of detrimental phases within the fusion zone – particularly coarse networks of Laves phase (Ni_2Nb) – and the dissolution of strengthening γ' and γ'' precipitates during the welding thermal cycle. Conversely, martensitic stainless steel displayed a base metal strength of 465 ± 5 MPa, while the welded joints reach 351 ± 25 MPa, corresponding to a joint efficiency of approximately 80%. The improved performance compared to INCONEL 718 was largely due to tempered martensite formation in the heat-affected zone (HAZ) and the absence of complex intermetallic phases that commonly challenge nickel-based superalloy welding.

The 0.2% offset yield strength presented distinct behaviours across the two alloys. For INCONEL 718, the base material measured 335 ± 10 MPa, while welded joints exhibited value of 273 ± 3 MPa. Optimal welding conditions (85 A current, 120 mm/min travel speed) produced yield strengths of 425 ± 18 MPa, which unexpectedly surpassed the base metal value (103%). This anomaly was linked to the formation of a fine dendritic structure and dispersion of carbides and nitrides in the fusion zone. In contrast, martensitic stainless steel showed a base yield strength of 290 ± 5 MPa, with weldments registering 445 ± 20 MPa under optimal conditions, equating to 86% of the parent metal. The observed reduction was primarily associated with untampered martensite in the HAZ and residual tensile stresses caused by phase transformation volume changes. Significant differences in ductility were observed between the two materials. Inconel 718 displayed 28% elongation in its base form, whereas welded joints showed a drop to 15–22%, influenced by heat input levels. The lowest ductility (15%) was recorded in specimens welded at higher heat input (100 A, 80 mm/min), which promoted excessive Laves phase formation and HAZ grain coarsening. Martensitic stainless steel, on the other hand, demonstrated 18% elongation in the base condition with weldments showing 12–16%, indicating a relatively smaller reduction. This was credited to a more uniform microstructure and absence of brittle intermetallic phases.

3.2.3. Fracture behaviour

Fractography revealed different failure mechanisms for the two materials. Inconel 718 specimens exhibited mainly transgranular fracture with dimpled rupture features, suggesting ductile fracture initiation followed by crack propagation through Laves phase networks. Secondary cracks were often located along grain boundaries within liquated regions of the HAZ. Martensitic stainless steel failures showed a mixed fracture mode, combining transgranular and intergranular characteristics. While the fusion zone displayed fine dimples indicative of ductile tearing, the HAZ exhibited some quasi-cleavage features associated with untempered martensite.

Table 5. Mechanical properties of Inconel 718 and AISI 410 dissimilar joints

Mechanical Property	Measure unit	Inconel 718	AISI 410	Welded joint
Yield Strength	MPa	335 ± 10	290 ± 5	273±3
Ultimate Tensile Strength	MPa	730 ± 10	465 ± 5	461 ± 2
Elongation	%	62 ± 2	25 ± 2	17.95 ± 0.8
Fracture Location	-		-	Parent metal of AISI 410

Based on the data, it's evident that joints noted a yield strength, ultimate tensile strength, and elongation. 273±3 MPa, 461 ± 2 MPa and 17.95 ± 0.8 %, respectively. Fracture occurred on the AISI material side (parent metal of AISI 410) during tensile testing, indicating that the strength of the welded zone in joints and TIG surpassed that of the AISI material. This superiority in strength was attributed to microstructural characteristics. The tensile measurements highlighted that the fusion zone demonstrated greater strength compared to the AISI 410 base metal.

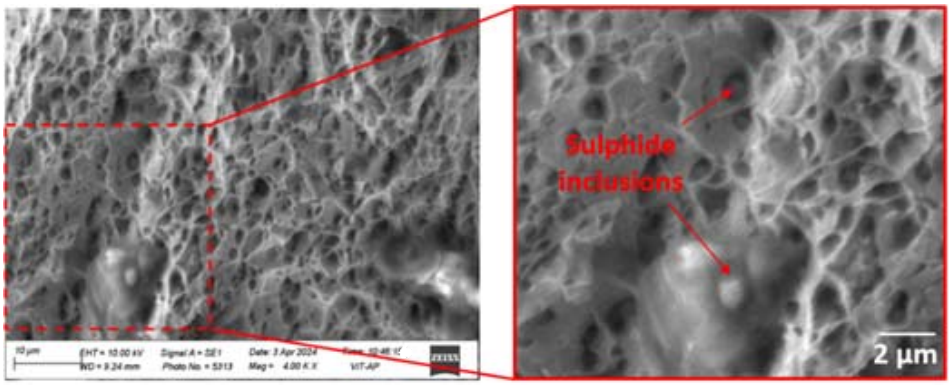

Fig. 7. Fractography of Inconel 718 and AISI 410 dissimilar joints

Figure 7 illustrates the fracture surfaces of the dissimilar joints from the tensile specimens. Both sets of specimens exhibited deep dimples and tear ridges, suggesting substantial energy absorption during dynamic deformation and fracture. SEM Fractography of the tensile-tested samples unveiled elliptically shaped sulphide inclusions (seen at higher magnification) composed of Mn and Fe. These inclusions likely played a role in initiating and propagating cracks during the tension test.

This study provides a direct, systematic comparison of TIG-welded Inconel 718 and AISI 410 dissimilar joints under identical process conditions, which fills an important gap in the literature. While several previous works examined either Inconel 718 or martensitic stainless steels independently or evaluated their welds in combination with austenitic stainless steels, few have directly contrasted the microstructural evolution and mechanical performance of these two alloys in a single experimental framework. This approach enables a deeper understanding of the unique challenges, phase transformations, and properties that arise at the dissimilar interface of Inconel 718 and AISI 410.

4. CONCLUSIONS

This study does not merely measure and catalogue properties; it clarifies how optimized TIG welding can overcome intrinsic challenges at the Ni-based superalloy/martensitic steel interface, and guides future engineering efforts for high-performance, dissimilar welded structures. These advances offer significant value for component reliability, safety, and design in demanding environments, and provide a robust reference for researchers and practitioners evaluating similar material systems.

The comparative assessment of TIG-welded Inconel 718 and AISI 410 martensitic stainless steel produced several key findings:

1. The welding process generated distinct microstructures on each material side. Inconel 718 exhibited dendritic solidification with Laves phase decorating dendrite cores, whereas AISI 410 presented coarse dendrites accompanied by interconnected sulphur inclusions within the fusion region.
2. Microhardness profiling revealed pronounced variation among different weld zones. The AISI 410 HAZ recorded the highest hardness value (410 HV) owing to martensitic transformation during rapid cooling. Inconel 718 maintained 267±3 HV in the base metal, with a slight reduction in its HAZ (247±4 HV), while the fusion zone displayed intermediate hardness (264±5 HV) due to mixed composition and refined dendritic structure.
3. The dissimilar welded joint achieved favourable strength characteristics, with an ultimate tensile strength of 461±2 MPa, supported by a yield strength of 273±3 MPa and elongation of 17.95±0.8%, indicating sufficient ductility for structural use. The consistent failure within the AISI 410 base metal rather than the weld area confirms that the fusion zone possessed higher strength compared to the weaker substrate.
4. Fractographic analysis predominantly revealed ductile fracture features, including deep dimples and tear ridges, suggesting substantial energy absorption before failure. Elliptically shaped sulphide inclusions- rich in Mn and Fe-acted as local stress concentrators, accelerating crack initiation and propagation under tensile stress rich in Mn and Fe-acted as local stress concentrators, accelerating crack initiation and propagation under tensile stress.

ACKNOWLEDGEMENTS

The authors wish to thank SASI Institute of Technology and Engineering for their constant support and encouragement in completing the research work

REFERENCES

[1] **Sonar T.**, **Balasubramanian V.**, **Nagar A.**, **Venkateswaran T.**, **Malarvizhi S.**, **Sivakumar D.**, *Microstructural characteristics and tensile properties of gas tungsten constricted arc (GTCA) welded Inconel 718 superalloy sheets for aeroengine components*, Materials Testing, 2020, vol. 62, iss. 11, pp. 1099-1108.

[2] **Sonar T.**, **Venkateswaran T.**, **Malarvizhi S.**, **Balasubramanian V.**, **Sivakumar D.**, *Effect of Heat Input on Evolution of Microstructure and Tensile Properties of Gas Tungsten Constricted Arc (GTCA) Welded Inconel 718 Alloy Sheets*, Metallography, Microstructure, and Analysis, 2020, vol. 9, iss. 3, pp. 369-392.

[3] **Mousazadeh M. A.**, **Derakhshandeh-Haghighi R.**, *Autogenous Tungsten Inert Gas Welding of 430 Ferritic Stainless Steel: The Effect of Inter-pass Temperature on Microstructure Evolution and Mechanical Properties*, Journal of Materials Engineering and Performance, 2020, vol. 29, iss. 12, pp. 7807-7820.

[4] **Sirohi S.**, **Świerczyńska A.**, **Rogalski G.**, **Landowski M.**, **Kumar N.**, **Pandey C.**, **Fydrych D.**, **Pandey S. M.**, *Microstructure and Mechanical Properties of Combined GTAW and SMAW Dissimilar Welded Joints between Inconel 718 and 304L Austenitic Stainless Steel*, Metals, 2022, vol. 13, iss. 1, p. 14.

[5] **Górka J.**, et al., *The effect of TIG welding on the structure and hardness of butt joints made of Inconel 718*, Heliyon, 2023, vol. 9, iss. 2, p. e13175.

[6] **Yelamasetti B.**, et al., *Mechanical characterization and microstructural evolution of TIG-welded Inconel 718/SS316L joints*, Journal of Materials Processing Technology, 2024, vol. 32, pp. 196–207.

[7] **Kumar D. V.**, *Dissimilar welding of nickel-based superalloy - A review*, Materials Science Forum, 2023, vol. 1090, pp. 1-15.

[8] **Hejripour F.**, et al., *Consumable selection for arc welding between stainless steel type AISI 410 and Inconel 718*, Journal of Manufacturing Processes, 2017, vol. 29, pp. 80-88.

[9] **Shehbaz T.**, et al., *Dissimilar tungsten inert gas welding between Inconel 718 and titanium*, Journal of Materials Engineering and Performance, 2022, vol. 31, iss. 5, pp. 4100-4112.

[10] **Yesudhasan B.**, **Ramesh Kannan C.**, **Senthilkumar N.**, **Manikandan D.**, **Deena Rose D.**, *Evaluating the TIG welding process mechanically and microstructurally in relation to welding parameters*, Proceedings of the Institution of Mechanical Engineers, Part E: Journal of Process Mechanical Engineering, 2024, https://doi.org/10.1177/09544089241283414

[11] **Park G.**, **Jeong B.**, **Lee M.**, **Kim J.-H.**, **Song S.**, **Park H. J.**, **Cha S. C.**, **Kim C. K.**, *Effect of Carburization on the Microstructure and Laser Weldability of 316L Stainless Steel*, Journal of Welding and Joining, 2023, vol. 41, iss. 6, pp. 475-485.

[12] **Manikandan S.**, **Kamaraj M.**, **Sivakumar D.**, **Rao K. P.**, *Effect of enhanced cooling on microstructure evolution of alloy 718 using the gas tungsten arc welding process*, Welding in the World, 2016, vol. 60, iss. 5, pp. 899-914.

[13] **Shit G.**, **Kuppusamy M. V.**, **Ningshen S.**, *Corrosion Resistance Behavior of GTAW Welded AISI type 304L Stainless Steel*, Transactions of the Indian Institute of Metals, 2019, vol. 72, iss. 12, pp. 2981-2995.